Investigation of Panel Crack Formation in Steel Ingots: Part I. Mathematical Analysis and Mid-Face Panel Cracks

B. G. THOMAS, I. V. SAMARASEKERA, and J. K. BRIMACOMBE

An investigation of panel crack formation in steel ingots has been undertaken to improve understanding of the mechanisms by which the cracks develop and to evaluate possible solutions to this problem that has plagued the steel industry intermittently for decades. The investigation features the application of two-dimensional, finite-element, heat-flow, and stress models, which have been described in earlier publications[1,2] for steel ingot processing. The model predictions have clarified the role of stress generation in panel crack formation and demonstrate the importance of the $\gamma \rightarrow \alpha$ phase transformation. It has been revealed that two distinct types of panel cracks, both of which are partly caused by intermediate-temperature embrittlement of steel involving aluminum nitride precipitation, operate under different mechanisms. Mid-face panel cracks, which are analyzed in Part I of this paper, apparently form during air cooling when the mid-face surface is between the Ar_1 and 500 °C. The cracks can be prevented by ensuring the ingot surface does not cool below the Ar_1, and preferably the Ar_3 temperature. In case of a 335 mm square ingot, this would require reheating and rolling within the first hour after being stripped from the mold. Alternatively charging the ingots to a holding furnace to slow the surface cooling rate through the critical Ar_1 – 500 °C temperature zone should be beneficial. Off-corner panel cracks are discussed in Part II.

I. INTRODUCTION

PANEL crack formation in static-cast steel ingots is a problem that has plagued the steel industry for several decades. Although the defect is intermittent and affects less than two percent of susceptible steel grades, the problem is persistent and expensive since affected ingots must be scrapped. Panel cracks are manifested as two distinct types of cracking problems, referred to as "mid-face" and "off-corner" panel cracks, respectively.[3] "Mid-face" panel cracks are found exclusively in small (1500 to 6000 kg), medium carbon (0.4 to 0.7 pct C), hypo-eutectoid, pearlitic steel ingots and usually exhibit a single, continuous, longitudinal fracture down the center of one of the ingot faces as shown in Figure 1.[3] Certain alloy steels are particularly prone to this defect and are affected at slightly lower carbon contents.[3,4]

"Off-corner" panel cracks often form rough oval, discontinuous, crack patterns on the wide faces of large (18,000 to 30,000 kg) ingots as seen in Figure 2.[4] They affect only low-carbon steels (0.1 to 0.2 pct C) with high Mn content (0.7 to 1.5 pct Mn) and are usually first observed when they open up during hot rolling. Both types of defect affect only killed, aluminum-treated steels (0.015 to 0.6 pct Al) and appear as deep, intergranular cracks that follow prior austenite grain boundaries.

In a previous review,[4] it was revealed that these cracks arise due to a combination of lowered intermediate temperature ductility and thermal stress generation. The loss of ductility in steel at intermediate temperatures has received a great deal of study which was reviewed as a preliminary step to the present investigation.[5] However, the generation of stresses in ingots arising from both changing thermal gradients and phase transformation is a complex subject that has received relatively little attention. Thus, the objective of the present investigation was to determine the mechanism(s) for panel crack formation, primarily through application of mathematical models developed to predict heat flow and stress generation in a static-cast ingot during the various processing stages prior to rolling.

B. G. THOMAS is Assistant Professor, Department of Mechanical and Industrial Engineering, University of Illinois at Urbana-Champaign, 1206 West Green Street, Urbana, IL 61081. I. V. SAMARASEKERA, Associate Professor, and J. K. BRIMACOMBE, Stelco/NSERC Professor and Director, are with The Centre for Metallurgical Process Engineering at the University of British Columbia, Vancouver, BC, Canada, V6T 1W5.

Manuscript submitted December 8, 1986.

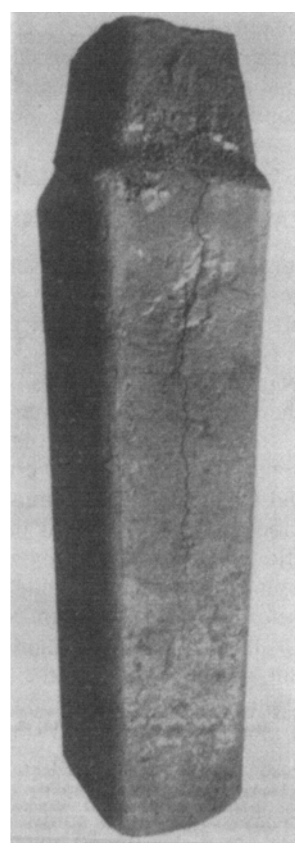

Fig. 1 — Mid-face panel crack in 350 × 350 mm square En18 (0.4 pct C, 1.0 pct Cr) steel ingot.[3]

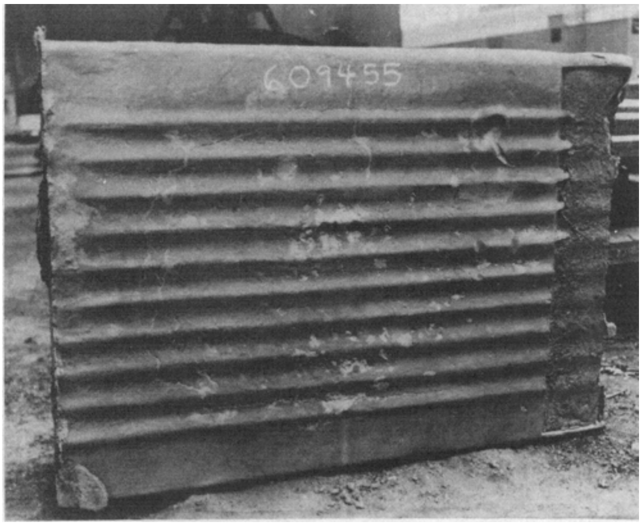

Fig. 2 — Off-corner panel cracks in a 760 × 1520 mm, rectangular, corrugated (0.14 pct C, 1.4 pct Mn, Si-killed, Al grain refined) steel ingot.[4]

Table I. Input Data for Model Simulation of Mid-Face Panel Cracks

Ingot size	355 × 355 mm
Steel composition	medium carbon steel 0.57 pct C, 0.65 pct Mn, 0.30 pct Si, 0.01 pct S, 0.01 pct P, 0.04 pct Al
Ar_1	650 °C
Ae_1	707 °C
Ac_1	720 °C
Ar_3	695 °C
Ae_3	747 °C
Ac_3	760 °C
Solidus temperature	1410 °C
Liquidus temperature	1480 °C
Initial steel temperature	1530 °C
Initial mold temperature	25 °C
Strip time (mold cooling time)	1800 s (30 min)
Initial time step size	0.9375 s
Maximum time step size	30 s

The models, which are described briefly in the next section, were applied to examine, separately, stress development in steel ingots processed under conditions conducive to the formation of mid-face and off-corner panel cracks. The generation of stresses which cause mid-face panel cracks in small ingots is described in Part I of this two-part paper. Stress development in larger ingots prone to off-corner panel cracks is presented in Part II together with a metallurgical investigation of these cracks. The results of the mathematical simulations, metallurgical investigation, and findings from previous studies are combined in both parts to propose mechanisms for the formation of each type of panel crack. Finally, solutions to the problems applicable to industry are proposed in the light of these mechanisms.

II. MATHEMATICAL HEAT FLOW MODEL

Since thermal stresses in the ingot arise solely from changing temperature gradients, the first step was to develop a mathematical heat-flow model to predict the thermal evolution of the solidifying steel. A detailed description of the formulation and computational procedure of this model has been given elsewhere.[1,6] Only one-quarter of a transverse, two-dimensional section through the ingot and mold at mid-height was considered, since panel cracks are primarily longitudinal and exhibit two-fold symmetry. The model simulates the various stages of thermal processing of the ingot through solidification and cooling in the mold, air cooling after stripping from the mold and, if necessary, reheating in a soaking pit and subsequent air cooling after withdrawal prior to hot rolling. It includes the variation in heat flow across the interface between the solidifying ingot skin and the mold due to air gap formation as a function of time and position along the ingot/mold surface.

For the problem at hand, steel property data input to the model were based on the composition given in Table I for a typical steel grade susceptible to mid-face panel cracks. The liquidus and solidus temperatures calculated based on this composition are also given in Table I while the other temperature-dependent thermal property data employed (conductivity, enthalpy, density, *etc.*) have been given previously.[1]

The model employs a version of the finite-element method to allow the incorporation of geometric features such as rounded corners and mold corrugations. Three-node, linear-temperature, triangular elements are used with temperature-dependent properties interpolated linearly within each element. The model has been verified through comparisons of the temperature predictions with both analytical solutions and temperatures measured during solidification of industrial steel ingots.[1]

Figure 3 shows the finite-element mesh employed to simulate thermal processing of a small, square 355 × 355 (14 in. × 14 in.), 2000-kg ingot which typically would be susceptible to mid-face panel cracks.

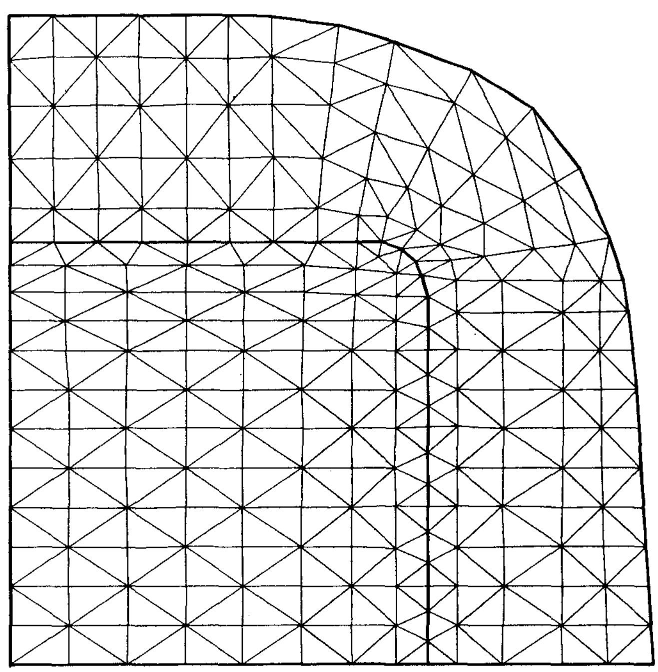

Fig. 3 — Finite element mesh for a 355 mm square, 2000 kg mid-face panel-cracked ingot and mold.

III. MATHEMATICAL STRESS MODEL

An uncoupled, two-dimensional, transient, elasto-visco-plastic, thermal stress model was developed to determine the internal stress state of the ingot arising from the changing temperatures calculated by the heat-flow model. The same one-quarter transverse section of the ingot was considered and stresses in the mold were not computed.

Details of the model formulation are given elsewhere;[2] thus only a brief description will be included here. The model incorporates the effects of temperature-dependent mechanical properties, plastic flow due to high-temperature creep, and volume changes due to phase transformations including the effects of kinetics. This is accomplished by dividing the total strain increment, $\Delta\varepsilon$, into three components:

$$\Delta\varepsilon = \Delta\varepsilon_e + \Delta\varepsilon_T + \Delta\varepsilon_p \qquad [1]$$

where $\Delta\varepsilon_e$ and $\Delta\varepsilon_T$ contain the elastic and thermal strain components, respectively. The creep and plastic strain components arising during each time step, Δt, were lumped together in $\Delta\varepsilon_p$ and calculated as a function of temperature, T, and Mises effective stress, $\overline{\sigma}$, from:

$$\Delta\varepsilon_p = \Delta t\dot{\varepsilon}_p(T, \overline{\sigma}_t) \qquad [2]$$

The "plastic-creep" functions, $\dot{\varepsilon}_p$, utilized to model typical medium- and low-carbon steels, representative of mid-face and off-corner panel cracks, respectively, were based on flow stress data from tensile tests conducted by Wray[7] on austenite at a plastic strain of 0.2 pct. To account for the enhanced creep rate of ferrite relative to austenite, the function for low-carbon steel was increased by a factor proportional to the phase fraction for temperatures extrapolated below the Ar_3 when ferrite is present.

Thermal strain was calculated incrementally as a function of the input temperatures over the time interval, by:

$$\Delta\varepsilon_T = TLE(T_{t+\Delta t}) - TLE(T_t) \qquad [3]$$

The volumetric expansion of roughly 1 pct that accompanies the $\gamma \rightarrow \alpha$ phase transformation has a significant effect on stress development within the ingot.[2] Thus, the overall thermal linear expansion function, *TLE*, for a given steel was calculated from a weighted average of *TLE* for the fractions of austenite, γ, and ferrite/pearlite, α, structures present. Thermal linear expansion functions for the individual phases were based on the temperature-dependent *TLE* functions of those respective phases in pure iron, modified to include the influence of carbon content on the expansion accompanying the $\gamma \rightarrow \alpha$ phase transformation.[8]

The kinetics of this phase transformation were also included by tracking the austenite fraction present during heating and cooling. The transformation is characterized by the start and finish temperatures on heating (Ac_1, Ac_3) and cooling (Ar_3, Ar_1) which are given in Table I for the steel affected by mid-face panel cracks. The values used to simulate medium-carbon steel for mid-face panel cracking were determined from CCT curves for a representative grade.[9] In addition to the literature data,[9,10] the values for low-carbon steel described in Part II were supplemented by dilatometer tests performed on specimens machined from an off-corner panel-cracked ingot.[8] Table I also includes the equilibrium transformation temperatures (Ae_3, Ae_1), which were calculated for the given compositions using equations adapted from Andrews.[8,11]

The stress model employs the finite-element method for spatial discretization, utilizing the mesh data from the heat-flow model as constant strain triangular elements. A simple, explicit time-stepping procedure based on the visco-plastic model of Zienkiewicz and Cormeau[13] was developed to solve for the displacement, strain, and stress fields at each time step of the simulation. Computational cost-saving features include use of the Choleski method to solve the banded, symmetric matrix equation, use of the same global conductivity (stiffness) matrix for several successive time steps, and variable time step sizes.[2]

The approach followed in running the stress model was to choose input data that maximized the effects of creep in order to isolate the unavoidable minimum stress level generated during thermal processing of the ingot. This was accomplished through the application of a plane-stress condition, the relatively low-valued function of Puhringer[12] for temperature-dependent elastic modulus, the relatively high valued function of Wray[7] for plastic-creep rate, and the relatively large enhancement of creep rate in ferrite of low-carbon steel by 1000× over that in austenite. Further details regarding the property data used and its implementation in the model are available in References 3 and 8.

IV. FRACTURE CRITERIA

Presentation of the results of a transient, two-dimensional, thermal stress model is made difficult by the vast amount of data generated. The task is linked to the problem of finding parameters that effectively quantify the stress state and adequately indicate the cracking potential. The total strain is largely composed of thermal strain which should not bear any direct influence on cracking tendency. On the other hand, inelastic strain due to plastic flow and creep should be a logical fracture criterion. For a creep void-coalescence fracture mechanism, both tensile and compressive inelastic strains contribute damage; consequently increments of inelastic or "plastic creep" strain were accumulated in a positive sense by

$$\overline{\varepsilon}_{p_{t+\Delta t}} = \overline{\varepsilon}_{p_t} + |\Delta\varepsilon_p| \qquad [4]$$

For materials that yield, flow plastically, and subsequently fail in a ductile manner, the Von Mises effective stress parameter, $\overline{\sigma}$, based on maximum distortion energy has been found to be a good fracture criterion.

$$\overline{\sigma} = (\sigma_x^2 + \sigma_y^2 + 3\tau_{xy}^2 - \sigma_x\sigma_y)^{1/2} \qquad [5]$$

However, regardless of their cause, cracks can propagate and open up only under tension. To distinguish regions of tension and compression, this parameter, $\overline{\sigma}$, was therefore assigned a negative value if the greatest principal stress was compressive. It is displayed graphically as iso-stress contour lines using a linear interpolation technique within elements. Temperature results are displayed in the same manner.

Finally, to visualize the simple fracture criterion of maximum normal stress, principal stresses, σ_{I}, σ_{II} were calculated

$$\sigma_{\mathrm{I,II}} = \frac{\sigma_x + \sigma_y}{2} \pm \left[\left(\frac{\sigma_x + \sigma_y}{2}\right) + \tau_{xy}^2\right]^{1/2} \qquad [6]$$

Because the columnar grain boundaries, growing perpendicular from the ingot surface, are known to be weak, the orientation of the stresses is also important. Therefore, the principal stresses were presented graphically as stress bars plotted at each node in the mesh. The bars are oriented in the directions of the principal stresses with lengths that are proportional to their magnitudes and compressive stresses are distinguished with tick marks at the end of each stress bar. When one of the principal stresses is aligned directly across the grain boundaries, it is referred to as the "normal stress".

Owing to the uncertainties involved both in calculating absolute stress levels based on incomplete mechanical property data and in determining adequate fracture criteria, the results of the numerical simulations are interpreted in a qualitative manner. Rather than attaching undue significance to the acutal stress values, the model predictions are used to focus attention on the location of tensile and compressive regions within the ingot and how they evolve over time. When combined with analysis of temperature predictions and knowledge of the elevated-temperature ductility of steel, mechanisms for panel crack formation can be developed.

V. MID-FACE PANEL CRACKS

The typical location of mid-face panel cracks in the transverse section of an ingot is shown in Figure 4.[3] The cracks run longitudinally down the center of as many as three of the four billet faces and can extend to depths of over one-quarter of the billet thickness. The defects are usually discovered either in the melt shop after stripping or during subsequent rolling operations. They are associated with excessive air cooling but their exact time of formation is unclear. Because the incidence of mid-face panel cracking increases with increasing aluminum and nitrogen contents, embrittlement from AlN precipitation is believed to play a major role in crack formation.[3,4,14] In addition, strain concentration in the primary ferrite at the austenite grain boundaries is thought to contribute to crack formation.[15]

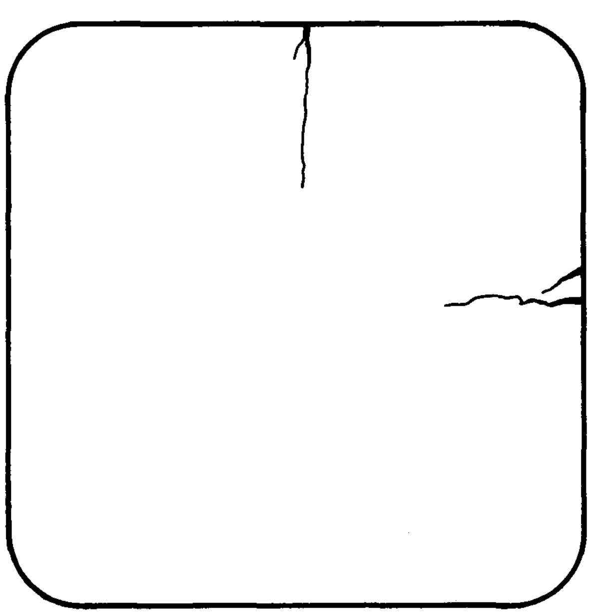

Fig. 4—Typical location of mid-face panel cracks in a transverse cross section of a 370 mm square, 0.55 pct C, steel ingot.[3]

Intergranular cracks then follow the ferrite networks between the pearlite grains along the prior austenite grain boundaries, producing a characteristic fracture surface of long, curved facets. Previous studies, therefore, identify metallurgical problems associated with the temperature range in which the $\gamma \rightarrow \alpha$ phase change occurs, as being primarily responsible for crack formation. The results from the mathematical simulations presented in the next sections shed light on the less studied, but nevertheless important, role of stress generation in contributing to the formation of mid-face panel cracks.

A. *Heat-Flow Model Predictions*

The heat-transfer model was used to simulate the development of temperature fields in both 355 mm and 405 mm square ingots processed under conditions where mid-face panel cracking might occur. Temperatures in the 355 mm ingot are presented in Figure 5 as contour plots through the transverse section at specific times during solidification in the mold and cooling in air. These results were obtained using the property data and processing conditions given in Table I. To summarize temperature development in that portion of the ingot where panel cracks are ultimately observed, Figure 6 presents temperature profiles for a slice taken through the center of this transverse section of the ingot.

During cooling in the mold, the smooth, evenly-spaced contours in Figure 5(a) show that temperature gradients within the thick, solidified shell are almost uniform. This is confirmed in Figure 6 which also shows the mushy ingot center resulting from early removal of the superheat. It is interesting to note, through a comparison of Figures 5(a) and 5(b), that the corner of the ingot reheats in the mold from a minimum of below 700 °C to over 850 °C by the time of stripping. This reheating phenomenon occurs, to a lesser extent, across the entire surface of the ingot and was encountered previously in large ingots.[1]

Very soon after stripping from the mold the ingot corner drops below the Ar_3 temperature of 695 °C as transformation to ferrite and pearlite begins. Eight minutes after stripping, the ingot has completely solidified and after this time, temperature gradients within the ingot reduce as the center cools more rapidly. Meanwhile, the corner has cooled below the Ar_1 of 650 °C and is completely transformed after 37 minutes of air cooling. With increasing time, the zone of transformation between the Ar_3 and Ar_1 isotherms spreads across the surface.

Figure 5(c) shows the progress of this transformation wave after one hour of air cooling, when it has passed almost completely beneath the ingot surface. Only the vicinity of the mid-face surface remains as two-phase material at this time. The transformation band then moves steadily inward and after 90 minutes of air cooling, the Ar_3 isotherm has just reached the ingot center, as indicated in Figure 5(d). By this time, the Ar_1 isotherm has moved over half the distance to the ingot center. The ingot center completes the $\gamma \rightarrow \alpha$ transformation six minutes later and further cooling continues to reduce temperature gradients within the ingot.

The heat-flow model results obtained when simulating the slightly larger 405 × 405 mm ingot were qualitatively identical. Only the time frame was expanded slightly as cooling was slower and the transformation front reached the various locations in the ingot at later times.

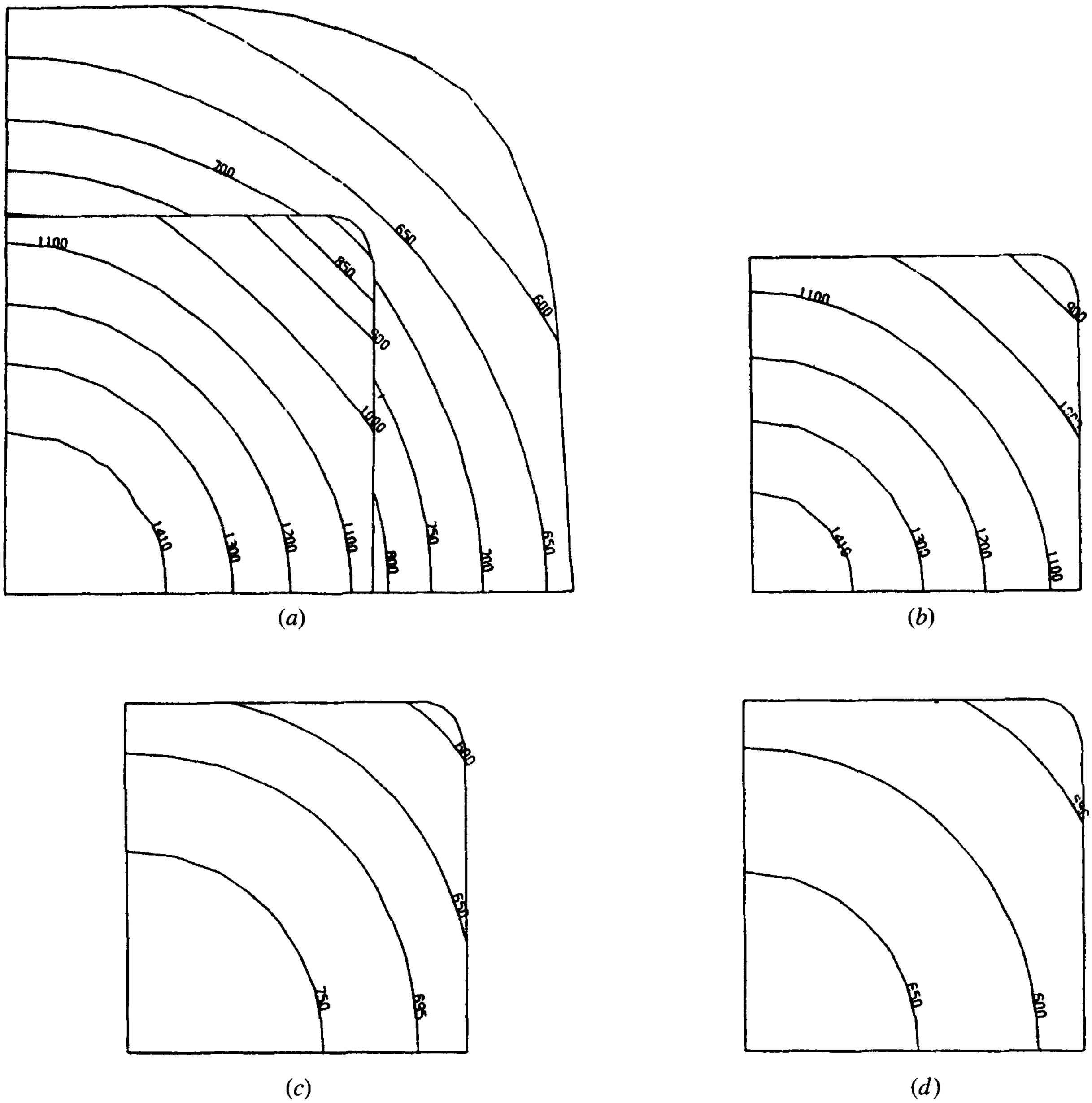

Fig. 5—Temperature contours (°C) calculated by heat-flow model for cooling of 355 mm square ingot: (*a*) conditions during mold cooling, 0.4 h after initial casting (1440 s); (*b*) conditions at strip after 30 min mold cooling (1800 s); (*c*) conditions during air cooling, 1 h after stripping (5400 s); and (*d*) conditions during air cooling, 1.5 h after stripping (7200 s).

B. *Stress Model Predictions*

Using the mechanical property data for medium-carbon steel, the stress model was run to predict stresses based on the temperature calculations for the processing of the 355 × 355 mm ingot just discussed. Figure 7 presents the results in the form of principal stresses. σ_I and σ_{II}, at each node in the transverse cross section of the ingot at several important times during air cooling. The same trends were also seen when examining contours of total effective stress, $\bar{\sigma}$; thus, for brevity the latter were omitted.

The importance of time in the development of the stresses can be more clearly seen through the simultaneous examination of Figures 7 and 8. Figure 8 tracks the progression of normal stress across the grain boundaries at two important locations: the mid-face surface, where the panel cracks ultimately penetrate, and a point 32 mm beneath. Thus solidification and cooling in the mold produce compression at the ingot exterior as the warm interior seeks to contract while cooling within a rigid outer framework that may be reheating. This surface compression persists well into air cooling, thereby preventing panel crack formation at the surface.

Throughout cooling in the mold, the ingot exterior remains in compression, thereby preventing panel crack formation at the surface. The slight tensile stress that develops beneath the surface is insufficient to generate internal cracks while in the mold for several reasons: (1) the low-sulfur steels affected by panel cracks have good ductility above 1000 °C; (2) the highest stresses are located

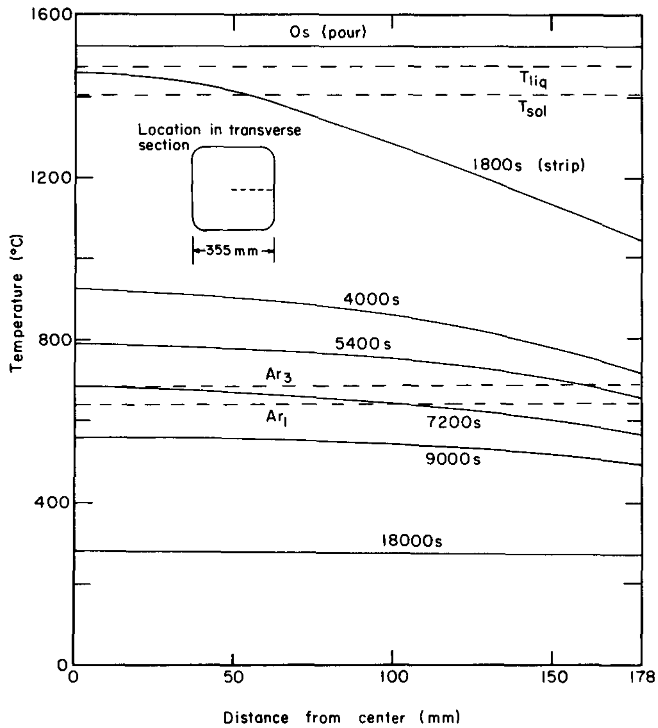

Fig. 6—Temperature profiles for slice through transverse section of 355 × 355 mm ingot calculated by heat-flow model at various times.

near the corner, far away from the ultimate location of the cracks; (3) the orientation of the stresses is parallel to the grain boundaries; (4) insufficient time has passed for detrimentral AlN precipitation in this region.

Immediately upon stripping, the contraction of the ingot surface, accompanying the rapid cooling, reduces the compressive stress at the surface. However, the surface soon falls into the two-phase $\gamma + \alpha$ region and starts to expand before any tension can develop. This occurs first at the corner, as seen in Figure 7(a), and then spreads across the surface, increasing in magnitude. Figure 7(b) illustrates the tangential band of hoop stresses that coincides with the two-phase $\alpha + \gamma$ region moving into the ingot.

The maximum compressive stresses are generated at the mid-face after one hour of air cooling (5400 seconds), as seen in Figure 8. The compressive peak always occurs when the temperature is just above the Ar_1. These compressive stresses induce complementary subsurface tensile stresses just inside the compressive band. The tensile peak across the grain boundaries is both low in magnitude and short-lived as these tensile stresses are oriented primarily in a radial direction. However, the temperature of the subsurface at this time which is just above the Ar_3 at 700 °C, coincides with a possible reduction in ductility at the low strain rates involved.[5] Thus, subsurface cracks might initiate in particularly susceptible steels even under this brief tensile stress. They would be prevented from propagating to the surface which remains in compression until 15 minutes later. This might explain the occasional presence of completely subsurface cracks.

The central core of the ingot is in a state of gradually increasing biaxial tension which reaches a peak level after 60 minutes of air cooling, as seen in Figure 7(b). Thirty minutes later, the compressive band has moved completely beneath the ingot surface into the central interior which reaches its maximum compressive stress shortly thereafter, as shown in Figure 7(c).

Meanwhile, the exterior of the ingot goes into tension, experiencing maximum tensile peaks at both surface and subsurface locations after one hour of air cooling, (7200 seconds), as seen in Figure 8. Tensile stress at this time is higher at the mid-face than anywhere else in the ingot at any time. This major tensile peak lasts a total of 45 minutes and coincides with the surface dropping below the Ar_1 temperature to transform completely to ferrite and pearlite. At the same time, the formation of a hard pearlite matrix surrounding weak ferrite networks could concentrate strain at the prior austenite grain boundaries, thereby reducing ductility. Further embrittlement would be caused by the rapid precipitation of fine AlN particles in the ferrite where it is less soluble. This combination of tensile stress and lowered ductility is expected to initiate panel cracks at the mid-face at this time. With further cooling, the tensile stresses generated both at the surface and below it would propagate the cracks deeper into the ingot.

The mid-face stays in tension until 9000 seconds, after roughly two hours of air cooling, as shown in Figure 8. At this time, a second band of compression spreads inward from the corner along the ingot surface. This coincides with the temperature falling to about 500 °C. Subsequently, neither the surface nor subsurface locations are ever in tension again.

However, this final compressive zone penetrates to a depth of only roughly one-third of the ingot thickness, leaving the interior with residual tensile stresses. The magnitude of the stresses steadily increases until the temperature within the ingot has completely equilibrated. Figure 7(d) shows the extent of this stress development after 4.5 hours of air cooling. This stress pattern approximates the residual stresses that persist even after the ingot has cooled to ambient temperature.

The residual compressive stresses at the surface would prevent any subsurface cracks from penetrating through to the surface that had not already done so. At the same time, the high internal tensile stresses would serve to propagate any existing cracks deep into the central core of the ingot. In addition, because the surface is tightly closed in compression by the time the ingot has cooled to ambient temperature, the extent of the damage might be difficult to perceive.

1. *Strain calculations*

Figure 9 represents contours of accumulated plastic-creep or inelastic strain, $\bar{\varepsilon}_p$, for the four critical times identified in the previous discussion. The maximum level of inelastic strain calculated by the stress model is always less than 2 pct. An examination of the literature on the hot ductility of steel[5] reveals that the minimum reduction in area values observed under severe embrittlement conductions rarely corresponds to less than 20 pct of the overall strain elongation. Even the most conservative methods for relating these values (which were determined under one-dimensional, isothermal test conditions), to the complex triaxial nonisothermal conditions within the ingot, predict a strain-to-failure higher than 2 pct. This result reveals that localized embrittlement and/or strain concentration at the prior austenite grain boundaries must be an essential feature in the mechanism of mid-face panel crack formation.

The pattern of plastic-creep strain contours that develops within the ingot by the time of stripping, shown in Fig-

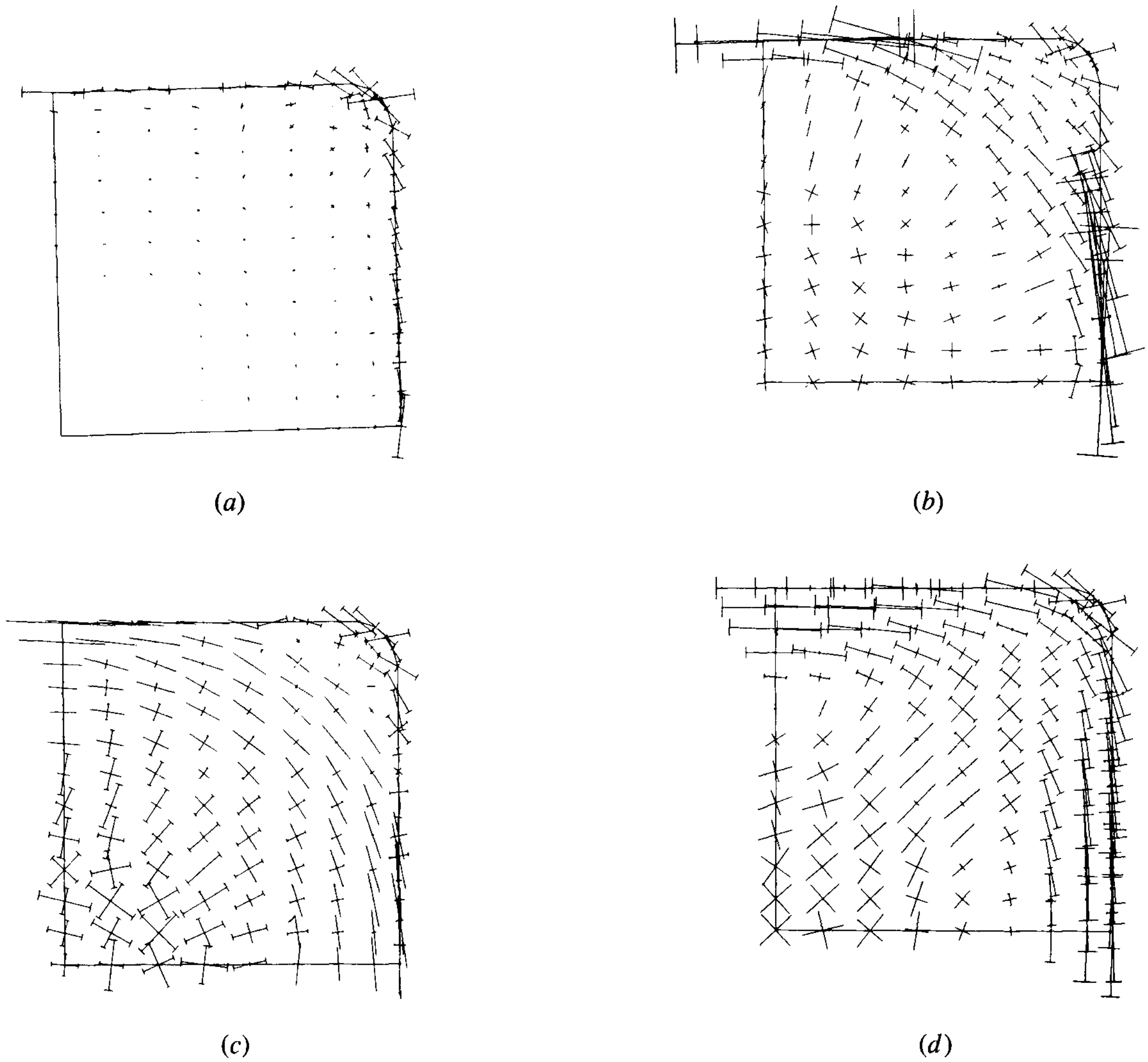

Fig. 7 — Principal stresses (MPa) calculated by stress model for simulated processing of 2 ton, 355 mm square ingot: (*a*) conditions at strip after 30 min mold cooling (1800 s); (*b*) conditions during air cooling, 60 min after strip (5400 s); (*c*) conditions during air cooling, 90 min after strip (7200 s); and (*d*) conditions during air cooling, 4.5 h after strip (18000 s).

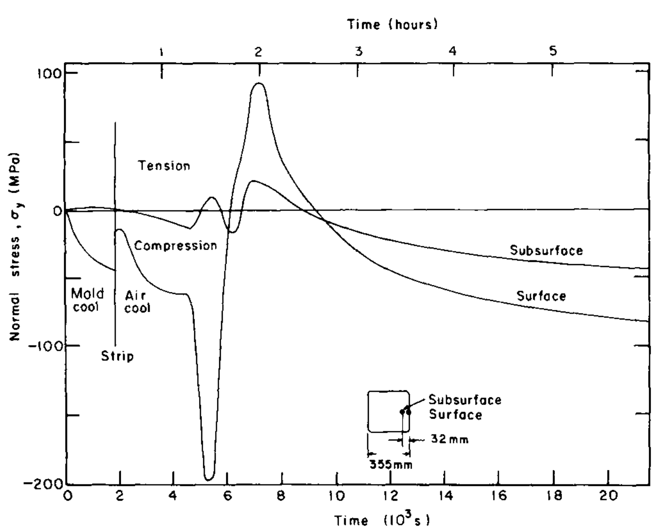

Fig. 8 — Stress histories of two important locations in 355 × 355 mm ingot during processing.

ure 9(a), remains essentially unchanged thereafter. The mid-face surface region always has the most inelastic strain, increasing from 0.3 pct at this time to almost 1.7 pct, 90 minutes later. Figures 9(b) and 9(c) illustrate the relatively large increase in accumulated inelastic strain of 0.5 pct that arises at the mid-face surface over the brief 30-minute time interval, corresponding to the rapid changes in stress state previously discussed. This finding further reinforces the previous prediction of crack formation at this location and time since this strain was accumulated within a temperature zone of embrittlement. Figure 9(d) shows that after 120 minutes, strain throughout the ingot changes very little, except at the central core which is still warm enough to creep.

Average plastic creep strain rates in the ingot, calculated from these results, range from 3×10^{-8} to 4×10^{-6} s^{-1}. Although the strain rate at the surface is initially considerably higher, reaching 1×10^{-4} s^{-1} early during mold cooling, it soon falls to a constant average rate of 3×10^{-6} s^{-1}. These low strain rates are detrimental to ductility.[5]

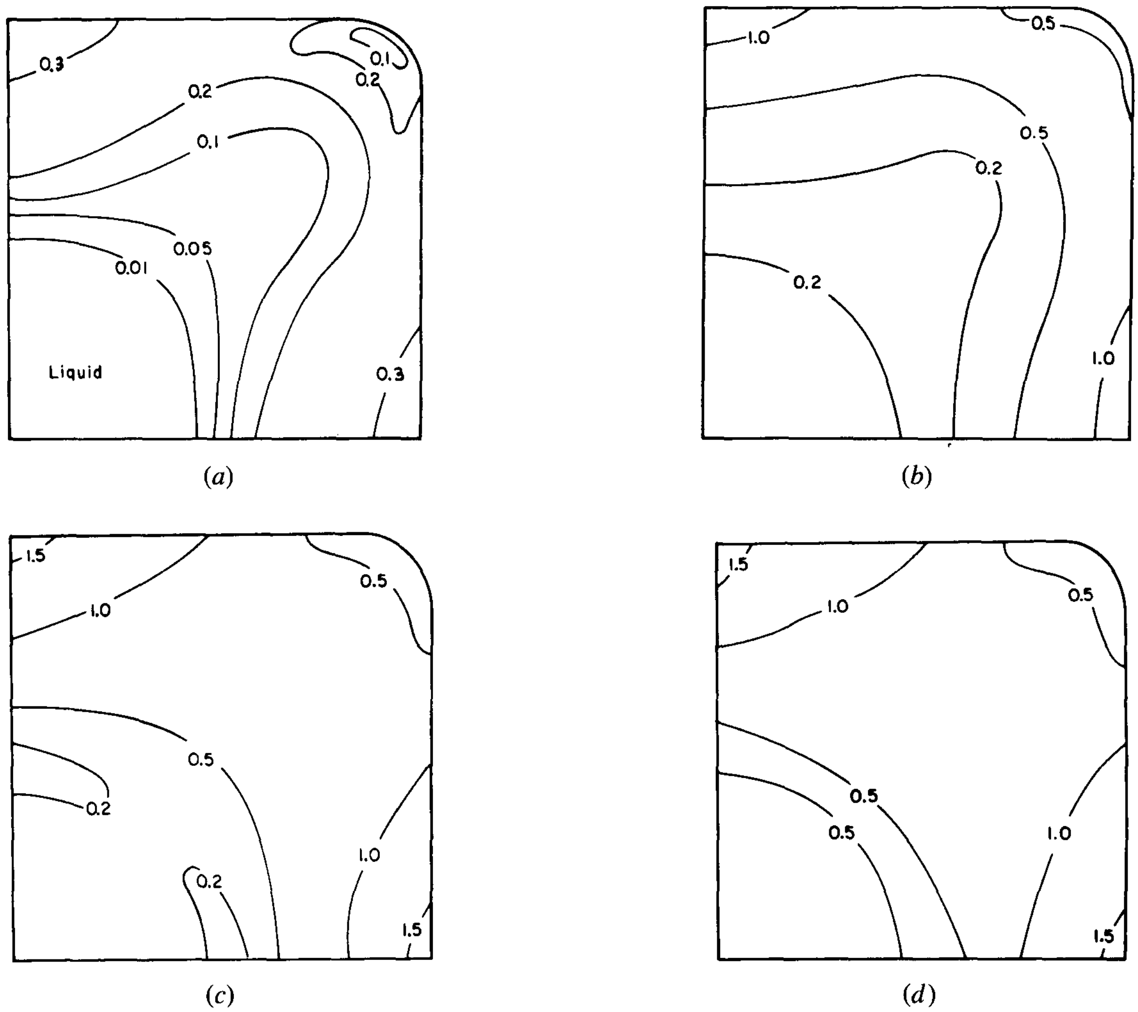

Fig. 9—Accumulated plastic-creep strain contours (pct) calculated by stress model for 355 × 355 mm ingot during air cooling: (*a*) conditions at strip after 30 min mold cooling (1800 s); (*b*) conditions during air cooling, 60 min after strip (5400 s); (*c*) conditions during air cooling, 90 min after strip (7200 s); and (*d*) conditions during air cooling, 4.5 h after strip (18000 s).

Figure 10 presents the stress-strain histories of the critical surface and subsurface locations. This figure exhibits essentially the same features as Figure 8 except that the compressive and tensile peaks are both extended, indicating the disproportionate amount of strain occurring during these critical times. The stress-strain history of the mid-face surface location is the most severe of any location in the ingot. The abrupt end of both curves indicates the lack of inelastic strain occurring after two hours of air cooling when both locations become cold and compressive.

2. *Effect of carbon content*

The effects of casting a low- instead of a medium-carbon steel on stress development in a 405 mm square ingot are shown in Figures 11(a) and (b) for the surface and subsurface locations, respectively. These figures essentially illustrate the influence of raising the Ar_3 temperature from 695 °C to 840 °C. The temperature histories of these locations are included in the figures as a means of locating the Ar_3 and Ar_1 temperatures that define the important phase change temperature interval, or PCTI.

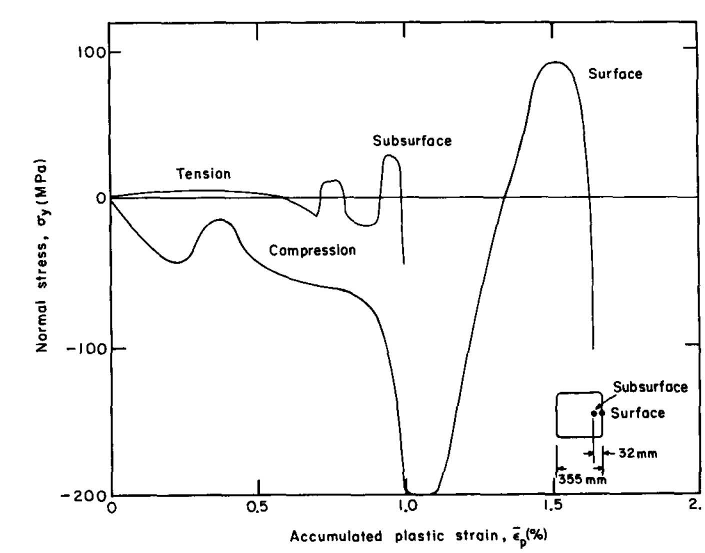

Fig. 10—Stress-strain histories for two important locations in 355 × 355 mm ingot during processing.

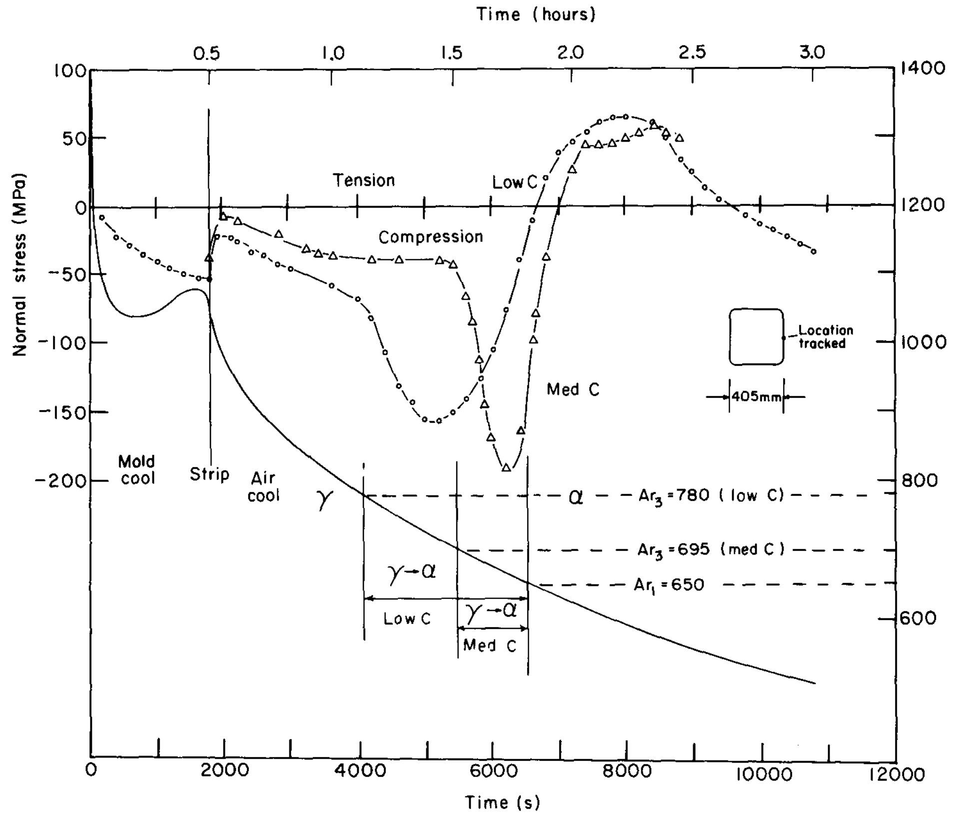

(*a*)

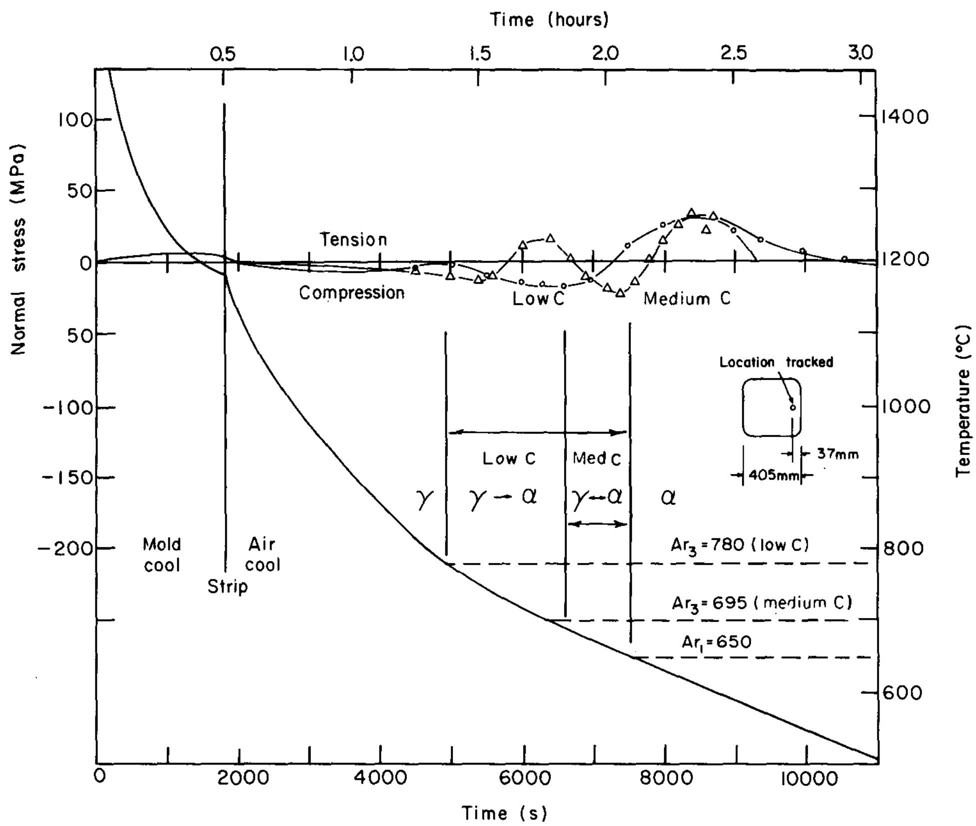

(*b*)

Fig. 11—Effect of carbon content of the steel on the thermal and stress histories of a 405 × 405 mm ingot during processing: (*a*) mid-face surface location and (*b*) mid-face subsurface location.

In general, different carbon contents produce similar stress-pattern development within the ingot. However, because the transformation starts at a higher temperature, events such as the shift from compression to tension at the surface tend to occur sooner in the low carbon steel. These results reflect how closely stress development is tied to the $\gamma \rightarrow \alpha$ phase transformation.

A second consequence of casting a low carbon steel, which has a wider $\gamma \rightarrow \alpha$ PCTI, is a compressive peak at the surface that evolves over a broader time span and reaches a smaller maximum magnitude. This results in a diminished effect on the adjacent interior. Figure 11(b) shows that the subsurface location for the low-carbon steel does not exhibit the first of the two tensile peaks found for the medium-carbon steel. This may be an additional factor explaining why mid-face panel cracks affect only medium-carbon steels. Finally, the maximum tensile stress achieved at the surface is larger for the low-carbon steel. This is probably due, in part, to the greater volume change between γ and α at lower carbon contents.

3. *Effect of ingot size*

The effect of increasing ingot size can be seen by comparing Figures 8 and 11. Qualitatively, there is little difference between stress development in these two ingots. However, stresses are generally lower in the larger ingot, most notably the compressive and tensile peaks at the surface. In addition, the times at which these critical events occur are later in the larger ingot. The peak compressive stress of -190 MPa is generated at 6300 seconds in the 405×405 mm ingot compared with -220 MPa at 5400 seconds in the 355×355 mm ingot; the peak surface tensile stress is 55 MPa at 8500 seconds for the larger ingot relative to 95 MPa at 7200 seconds in the smaller ingot. In other respects, these two ingots behave in a very similar manner.

Based on the results of the stress model alone, smaller ingots would generally be expected to experience a slightly greater tendency for mid-face panel cracking, owing to their slightly higher maximum stresses. However, because smaller ingots also experience the thermal and stress events sooner, mid-face panel cracking may be avoided in very small ingots when the surface tensile peak subsides before a sufficient amount of AlN precipitation has taken place to embrittle the grain boundaries. For ingots larger than this critical size, incidence of mid-face panel cracking should decline with increasing ingot size. This agrees with the observations of Erickson[16] and might explain why mid-face panel cracks are not found in very large ingots.

C. *Mechanism of Crack Formation*

The results of the stress model simulations, combined with knowledge of elevated-temperature zones of embrittlement in steel, lead to a consistent mechanism for the formation of panel cracks at the mid-face of small, medium-carbon ingots. During cooling, this critical surface location first experiences the highest compressive stresses. The resultant high shear could contribute to grain boundary weakening. Subsequently, the mid-face experiences the highest tensile stress of any location in the ingot. This is combined with a dramatic increase in inelastic strain, which is also the highest at this location. The maximum principal tensile stress acts directly across the grain boundaries which is the most detrimental orientation for grain boundary fracture. The critical temperature range over which this single, major, tensile peak is experienced is between the Ar_1 and 500 °C which falls directly in a lower-temperature zone of embrittlement for steel.[5] In this zone, the ferrite networks are surrounded by pearlite and sufficient time has passed for the low strain-rate void coalescence of nitride precipitates in the prior-austenite-grain-boundary ferrite. All of these factors indicate that the time of mid-face panel crack formation corresponds to this tensile peak when the mid-face surface is between 500 °C and the Ar_1.

The stress model predictions also suggest that larger ingots should be less prone to mid-face panel cracking, owing to their lower levels of maximum tensile stress. In addition, lower carbon steels should be less susceptible owing to their less severe stress development, their lack of a preliminary subsurface tensile peak, and the absence of a hard pearlite matrix surrounding ferrite networks below the Ar_1 temperature. These predictions agree with most of the hypotheses and findings of previous researchers.[15,17,18]

D. *Solutions*

This mechanism suggests a number of different methods for preventing mid-face panel crack formation. The first of these is to prevent the ingot surface from cooling below the Ar_1 temperature and thus avoids the high tensile peak. To ensure that subsurface cracks also do not form, it would be preferable to prevent the mid-face surface from falling below the Ar_3. This could be achieved by reheating and rolling 335 mm square ingots within the first hour after stripping.

Alternatively, slow, controlled cooling through the critical temperature range might alleviate the problem by delaying and reducing the magnitude of the tensile peak. This agrees with the findings of previous workers that slow cooling alleviated cracking problems.[14,16] It is interesting to note that the cooling rate experienced by the ingot while the mid-face surface is below 500 °C is inconsequential since the surface is in compression by that time. Thus, charging the ingots into a holding furnace for a short time while the ingot surface cools to below 500 °C should be sufficient to prevent mid-face panel-crack formation. Longer cooling in the holding furnace is unnecessary. Alternatively, laying one face of the ingot on an insulating surface, as proposed by Guerin,[17] should also reduce stress generation by concentrating strain in the single hot face above the Ar_3 temperature. This would again reduce the magnitude of the tensile peaks experienced by the ingot mid-face and reduce the likelihood of crack formation.

The final solution to mid-face panel cracking is simply to avoid the production of steel compositions susceptible to a low temperature zone of embrittlement. This requires the lowering of aluminum or nitrogen contents or using an alternative grain refiner. Unfortunately, the same mechanism that causes grain boundary embrittlement leading to panel-crack formation is also responsible for the beneficial grain refinement effects so desirable in later processing.[5] Thus, the application of this solution requires the possible acceptance of inferior low temperature properties such as impact toughness.

VI. SUMMARY AND CONCLUSIONS

The mathematical model predictions of temperature and stress evolution in small square ingots, in combination with a knowledge of elevated-temperature low ductility of steel, clearly reveal the mechanism of formation of mid-face panel cracks. It has been found that the $\gamma \rightarrow \alpha$ phase transformation plays a major role.

During air cooling after the ingot has been stripped, the progress of the two-phase, $\alpha \rightarrow \gamma$ transformation region, which moves into the ingot from the surface, is accompanied by a zone of high compression. This zone is followed by a complementary tensile region whose subsequent contraction gradually builds a peak of high tension between the Ar_1 and 500 °C before subsiding into compression again. In small square ingots the maximum tension occurs at the mid-face where it may concentrate strain at AlN-embrittled, pro-eutectoid ferrite networks that initiates cracks at the surface along prior-austenite grain boundaries. In addition, the narrow $\gamma \rightarrow \alpha$ PCTI of higher carbon steels produces a preliminary subsurface tensile peak that might account for internal mid-face panel cracks. The higher stress levels produced in smaller ingots make them more susceptible to crack formation by this mechanism. With further cooling, the relative contraction of the interior of the ingot accompanying the general leveling off of temperature gradients produces high internal tensile stresses that propagate these cracks deep into the ingot.

These findings suggest several solutions to mid-face panel cracking:

1. Prevent the mid-face surface from dropping below the Ar_3 temperature around 700 °C by reheating the ingot prior to excessive cooling.
2. Reduce tensile stresses over the critical temperature range between 500 °C and the Ar_1 temperature by slow or asymmetrical cooling.
3. Prevent the formation of ferrite networks and embrittling nitride precipitates by producing less susceptible steel compositions.

NOMENCLATURE

Ac_1, Ac_3	Austenite to ferrite transformation start and end temperatures on heating (°C)
Ar_3, Ar_1	Austenite to ferrite transformation start and end temperatures on cooling (°C)
Ae_3, Ae_1	Equilibrium transformation temperatures
t	Time (s)
T	Temperature (°C)
TLE	Thermal linear expansion
x, y	Coordinate directions (m)
ε	Strain (mm mm^{-1})
$\dot{\varepsilon}_p$	Plastic-creep function
$\overline{\varepsilon}_p$	Positively accumulated total effective plastic-creep strain (mm mm^{-1})
ε_p	Plastic (and creep) component of strain (mm min^{-1})
ε_T	Thermal component of strain (mm mm^{-1})
σ	Stress (MPa)
$\overline{\sigma}$	Von Mises effective stress parameter (MPa)
σ_{I}, σ_{II}	Principal stresses (MPa)
τ_{xy}	Shear stress (MPa)

REFERENCES

1. B.G. Thomas, I.V. Samarasekera, and J.K. Brimacombe: *Metall. Trans. B*, 1987, vol. 18B, pp. 119-30.
2. B.G. Thomas, I.V. Samarasekera, and J.K. Brimacombe: *Metall. Trans. B*, 1987, vol. 18B, pp. 131-47.
3. B.L. Biggs: *J. Iron Steel Inst.*, 1959, vol. 197, pp. 361-77.
4. B.G. Thomas, J.K. Brimacombe, and I.V. Samarasekera: *I.S.S. Trans.*, 1986, vol. 7, pp. 21-29.
5. B.G. Thomas, J.K. Brimacombe, and I.V. Samarasekera: *I.S.S. Trans.*, 1986, vol. 7, pp. 7-20.
6. B.G. Thomas, I.V. Samarasekera, and J.K. Brimacombe: *Metall. Trans. B*, 1984, vol. 15B, pp. 307-18.
7. P.J. Wray: *Modeling of Casting and Welding Processes*, H.D. Brody and D. Apelian, eds., TMS, 1980, pp. 245-57.
8. B.G. Thomas: Ph.D. Thesis, The University of British Columbia, Vancouver, BC, Canada, 1985.
9. M. Atkins: *Atlas of Continuous Cooling Transformation Diagrams for Engineering Steels*, British Steel Corporation, Sheffield, 1977.
10. C.F. ZurLippe and J.D. Grozier: *Metal Progress Data Sheet*, Feb. 1969.
11. K.W. Andrews: *J. Iron Steel Inst.*, 1965, vol. 203, p. 721.
12. O.M. Puhringer: *Stahl und Eisen*, 1976, vol. 96, no. 6, pp. 279-84.
13. O.C. Zienkiewicz: *Int. J. Numer. Methods in Eng.*, 1974, vol. 8, pp. 821-45.
14. B.C. Desai: *J. Iron Steel Inst.*, 1959, vol. 197, pp. 250-56.
15. K.J. Irvine and F.B. Pickering: *Iron and Steel*, June 1957, pp. 219-23.
16. L. Erickson: *Scand. J. Metallurgy*, 1977, vol. 6, pp. 116-24.
17. J.F. Guerin and C.M. Roccatagliata: *Siderurgia*, 1975, vol. 2, no. 6, pp. 91-108.
18. Hajime Nashiwa, K. Ozaki, M. Yoshihara, and H. Takashima: *Tetsu-to-Hagané*, 1976, vol. 62, no. 4, p. S156. (Translation by Center for Research Libraries No. CRL/T. 7004.)